AD_____

Award Number: DAMD17-00-1-0677

TITLE: MR Elastography System for Breast Cancer Detection

PRINCIPAL INVESTIGATOR: Robert J. Kline-Schoder, Ph.D.
                        Marc A. Kenton

CONTRACTING ORGANIZATION: Creare Incorporated
                          Hanover, New Hampshire 03755

REPORT DATE: October 2001

TYPE OF REPORT: Annual

PREPARED FOR: U.S. Army Medical Research and Materiel Command
              Fort Detrick, Maryland 21702-5012

DISTRIBUTION STATEMENT: Approved for Public Release;
                        Distribution Unlimited

The views, opinions and/or findings contained in this report are
those of the author(s) and should not be construed as an official
Department of the Army position, policy or decision unless so
designated by other documentation.

REPORT DOCUMENTATION PAGE

1. AGENCY USE ONLY (Leave blank)	2. REPORT DATE October 2001	3. REPORT TYPE AND DATES COVERED Annual (30 Sep 00 – 30 Sep 01)

4. TITLE AND SUBTITLE
MR Elastography System for Breast Cancer Detection

5. FUNDING NUMBERS
DAMD17-00-1-0677

6. AUTHOR(S)
Robert J. Kline-Schoder, Ph.D.
Marc A. Kenton

7. PERFORMING ORGANIZATION NAME(S) AND ADDRESS(ES)
Creare Incorporated
Hanover, New Hampshire 03755

E-Mail: rjk@creare.com

8. PERFORMING ORGANIZATION REPORT NUMBER

9. SPONSORING / MONITORING AGENCY NAME(S) AND ADDRESS(ES)

U.S. Army Medical Research and Materiel Command
Fort Detrick, Maryland 21702-5012

10. SPONSORING / MONITORING AGENCY REPORT NUMBER

11. SUPPLEMENTARY NOTES
Report contains color

12a. DISTRIBUTION / AVAILABILITY STATEMENT
Approved for Public Release; Distribution Unlimited

12b. DISTRIBUTION CODE

13. ABSTRACT *(Maximum 200 Words)*

Early diagnosis of breast cancer, which is critical for favorable clinical outcomes, is difficult because of the need to detect small tumors. One physical property that clearly distinguishes healthy from cancerous tissue is mechanical stiffness or hardness. Researchers have attempted to combine external mechanical stimulation and Magnetic Resonance Imaging (MRI) to quantitatively measure the Young's modulus of tissue throughout both the breast and the prostate. This technique, Magnetic Resonance Elastography (MRE) has been called "palpation at a distance."

One of the most challenging technical aspects of MRE is the solution of the "inverse problem," i.e., quantitatively determining Young's modulus from MRI-measured tissue displacement data. Creare is developing analytical solution techniques to improve the efficiency and robustness of the inverse problem solution. One technique, which combines an adjoint method for calculating the gradient of the goodness-of-fit metric combined with a quasi-Newton algorithm, appears to provide a substantial improvement in efficiency. We are also investigating improvements in the physical modeling on which the inverse method is based, primarily in the representation of tissue compressibility.

14. SUBJECT TERMS
Breast Cancer, elastography, MRI, inverse problem

15. NUMBER OF PAGES
23

16. PRICE CODE

17. SECURITY CLASSIFICATION OF REPORT	18. SECURITY CLASSIFICATION OF THIS PAGE	19. SECURITY CLASSIFICATION OF ABSTRACT	20. LIMITATION OF ABSTRACT
Unclassified	Unclassified	Unclassified	Unlimited

Creare

FOREWORD

Opinions, interpretations, conclusions and recommendations are those of the author and are not necessarily endorsed by the U.S. Army.

( ) Where copyrighted material is quoted, permission has been obtained to use such material.

( ) Where material from documents designated for limited distribution is quoted, permission has been obtained to use the material.

( ) Citations of commercial organizations and trade names in this report do not constitute an official Department of the Army endorsement or approval of the products or services of these organizations.

( ) In conducting research using animals, the investigator(s) adhered to the "Guide for the Care and Use of Laboratory Animals," prepared by the Committee on Care and Use of Laboratory Animals of the Institute of Laboratory Animal Resources, National Research Council (NIH Publication No. 86-23, Revised 1985).

( ) For the protection of human subjects, the investigator(s) adhered to policies of applicable Federal Law 32 CFR 219 and 45 CFR 46.

( ) In conducting research utilizing recombinant DNA technology, the investigator(s) adhered to current guidelines promulgated by the National Institutes of Health.

_____   _____
Principal Investigator's Signature   Date

TABLE OF CONTENTS

**Progress Report on the MR Elastography System
for Breast Cancer Detection**

1.0 INTRODUCTION

Breast cancer is the most commonly diagnosed cancer in women. Early diagnosis, which is critical for favorable clinical outcomes, is complicated by the difficulty of detecting small tumors. One physical property that clearly distinguishes healthy from cancerous tissue is mechanical stiffness (hardness). For this reason, palpation has long been used for early screening. Researchers have attempted to combine external mechanical stimulation and Magnetic Resonance Imaging (MRI) to quantitatively measure the Young's modulus of tissue throughout both the breast and the prostate. This technique, Magnetic Resonance Elastography (MRE) has been called "palpation at a distance." One of the most challenging technical issues of MRE is the solution of the "inverse problem," i.e., quantitatively inferring Young's modulus from MRI-measured tissue displacement data. Addressing this problem was the focus of Creare's efforts in the first year of this project.

2.0 BACKGROUND

Breast cancer is the most commonly diagnosed cancer in women, with a current mortality rate of approximately 23 per 100,000. Early diagnosis, which is critical for favorable clinical outcomes, is complicated by the difficulties associated with detecting small tumors. While mammography is very useful, the X-ray attenuation properties of tumors and normal tissues are similar, often making it difficult to distinguish small tumors from healthy tissue. The same problems afflict ultrasound, since the acoustic impedance of tumors is only slightly different from that of normal tissue.

One physical characteristic that does clearly distinguish healthy from cancerous tissue is mechanical stiffness (hardness). The Young's modulus of breast tumors can be one to two orders of magnitude larger than that of normal tissue (Muthupillai and Ehman, 1996). For this reason, palpation has long been used by physicians and patients for early screening. However, manual palpation is not very effective for tumors lying deep within the breast and is not quantitative. For these reasons, over the past decade, numerous efforts have been underway to combine external mechanical stimulation and various imaging techniques to quantitatively measure the Young's modulus of tissue throughout both the breast and the prostate. This has been termed "palpation at a distance." Because of its inherent sensitivity, much current research is focused on using magnetic resonance imaging (MRI), and the overall process is termed magnetic resonance elastography (MRE).

Probably the most challenging technical aspect of MRE is the solution of the "inverse problem," i.e., quantitatively inferring Young's modulus from MRI-measured tissue displacement data (Trahey, 2001). Addressing this problem was the focus of Creare's efforts in the first year of this project.

2.1 PREVIOUS WORK

A number of researchers have investigated use of displacement images to infer the Young's modulus of tissue. Early work focused on utilizing ultrasound images, but much

current research employs MRI which can accurately measure much smaller displacements (less than one micron) and has higher resolution than ultrasound.

MRE techniques can be broadly distinguished by whether they employ static or dynamic displacement of the tissue surface. Static techniques measure the change in tissue displacement resulting from a quasi-static push on the outside of the breast, or a sequence of pushes. This method is, in principle, simpler than dynamic methods, but certain mathematical difficulties arise from the use of static displacements. These difficulties appear to have led to the virtual abandonment of this technique (Raghavan and Yagle, 1994; Chenevert et al. 1998; Skovoroda et al. 1995).

Dynamic MRE usually involves the generation of oscillatory motions at the surface of the breast to induce shear waves in the tissue. Because shear waves are strongly attenuated, researchers have also investigated the use of ultrasound to induce shear waves in deep tumors via longitudinal/shear mode conversion (Wu et al. 2000). In either case, the motion of the interior of the breast (or phantom) is then measured using MRI, and the elastic modulus is inferred from these measurements.

MRE requires the use of relatively low excitation frequencies since motion at more than about 1 kHz cannot be resolved by MRI. Shear waves are used, because even at these low frequencies they have a sufficiently short wavelength to allow the resolution of small features such as tumors. Longitudinal waves have a much faster sound speed, a correspondingly larger wavelength, and thus little resolving power.

Two techniques have been used to infer Young's modulus from shear-wave-induced displacement data. Early research efforts employed direct measurements of the wavelength of shear waves at various points in a tissue phantom to determine shear wave speed. From shear wave speed, the modulus can be readily determined (Muthupillai et al. 1995; Manduca et al. 1996). A difficulty of this direct technique is that in real tissue, acoustic waves scatter off tissue inhomogeneities and the scattered waves interfere, generally leading to a very complex pattern of displacements (van Houten et al. 1999). Such a complex pattern does not lend itself to direct measurements of wavelength. To avoid this problem, several researchers have turned to physics-based modeling of tissue motion. In this method, the equations of motion of the tissue are defined in terms of the known oscillatory boundary conditions and a set of assumed tissue properties (i.e., Young's modulus). These equations are then solved, usually with finite element techniques, and then the calculated displacement patterns are compared to those measured with MRI. The assumed Young's moduli in the model are then systematically altered and the process repeated until the predicted and measured displacement patterns match (to within some tolerance).

One of the most active groups pursuing this approach is at Dartmouth College's Medical School and Thayer School of Engineering. They have reported substantial success, but two key problems stand out:

1. The time required to converge the inverse calculations can be measured in days, even for a relatively coarse mesh on a high-performance workstation. While this has led to the development of so-called subzone techniques and utilization of parallel processing to reduce execution times, this continues to represent a significant practical problem for using MRE in a clinical setting (Van Houten et al. 1999; Van Houten, et al. 2000a).

2. While good results have been reported in numerical simulations, the results in real tissue and in phantoms have been decidedly mixed. This has lead to recent efforts to model transient effects (rather than assuming steady-state), motion in three dimensions (rather than the plane strain approximation used previously), and speculation that viscoelastic behavior may need to be modeled (Van Houten et al. 2000b).

2.2 OVERVIEW OF CREARE EFFORTS

Creare efforts to date have focused primarily on reducing the time required to solve the inverse problem. Further, our most recent efforts have begun to address how to increase the fidelity of the reconstruction process (i.e., the underlying finite element model). In this section, we will introduce these areas of research. The next two sections will describe our work in more detail.

The Dartmouth group obtains updated Young's modulus estimates by minimizing the following figure of merit of the results:

$$J = \sum_{i=1,.n} (u_i - u_i^o)^2 + (v_i - v_i^o)^2 \tag{1}$$

In Equation (1), u and v denote the x- and y-direction displacements at each of the n nodes of the model at some specified time in their oscillatory cycle. The superscript "o" denotes displacements obtained from measured MRI data (which can come from an actual MRI or from a finite element simulation). The lack of a superscript denotes code-calculated displacements based on the current estimate for Young's modulus at each node. Note that in this and the following discussion, we assume that a two-dimensional, plane strain approximation is adequate, although the formulation can be readily generalized to a full 3-D analysis. We will later briefly discuss a modeling possibility that may alleviate the need to consider a fully three-dimensional analysis.

The Dartmouth group minimizes J using a well-known technique known as the Levenberg-Marquardt algorithm (Press et al. 1986). This requires the estimation of the Hessian matrix associated with J, which in turn requires the calculation of terms such as:

$$\frac{\partial u_i}{\partial E_k} \text{ and } \frac{\partial v_i}{\partial E_k} \quad i=1,...n; k=1,...p \tag{2}$$

where E_k denotes the Young's modulus of the kth element in the finite element model. If there are n nodes in the model, the calculation of the nodal displacements requires a time proportional to roughly n^3. However, the calculation of the terms (2) requires a time that is p times longer than this, which for low order elements (for which p is roughly equal to n) is on the order of n^4. This is a significant disadvantage as the number of elements and nodes grows unless the

calculation of these quantities makes convergence to the proper Young's modulus distribution much more rapid.

Since the time required to calculate the terms in the approximate Hessian matrix is very long, we have investigated the use of a quasi-Newton method, specifically the Boyden-Fletcher-Goldfarb-Shanno (BFGS) algorithm (Press et al. 1986). While this method is likely to require more iterations to converge than Levenberg-Marquardt, BFGS requires the calculation of only the gradient of the figure-of-merit, i.e., the terms:

$$\frac{\partial J}{\partial E_k} \quad k=1,\ldots p \tag{3}$$

To facilitate use of this technique, we developed an algorithm that very efficiently calculates the terms of the gradient. This algorithm is described in Section 2.3.

When we employed tissue mechanical properties similar to those used in the literature in numerical experiments, we achieved good success in estimating the values of the Young's modulus from simulated displacement data. We subsequently determined that much of the work reported in the literature appears to use a value for Poisson's ratio that can severely distort the results. We are currently working to remedy this problem. These efforts are described in Section 2.4.

2.3   IMPROVED INVERSE SOLUTION TECHNIQUES

2.3.1   Solution of the Tissue Equations of Motion

To develop an improved inverse solution technique, it is first necessary to develop a numerical model for the tissue displacements given an assumed set of tissue properties. While a commercial product such as ANSYS can (and was) used for preliminary analyses (see Section 2.4), ultimately a customized computer code is needed so that the displacement solution can be integrated with the solution of the inverse problem. We developed a finite element code in Fortran 90 for this purpose using the techniques outlined in Smith and Griffiths (1998). One design goal was to construct a code that would be capable of handling relatively large problems so that this code could serve as a test bed to investigate techniques for accelerating the solution of very large MRE inverse problems.

The finite element code calculates the steady-state amplitude of a damped, linear elastic solid in plane strain, subjected to a sinusoidal shear or longitudinal displacement along one or more edges. The mesh is generated by a separate program written for this purpose and read from a file. Various types of elements can be used, including triangles and quadrilaterals of various numbers of nodes.

In terms of the development of a finite-element model, the equations of motion of the nodes of the model can be written:

$$KM\,\bar{u} + \beta KM\,\frac{d\bar{u}}{dt} + MM\,\frac{d^2\bar{u}}{dt^2} = \bar{F} \tag{4}$$

where

$\overline{u}$ = time-dependent displacement vector of the nodes
KM = stiffness matrix (relates displacements to stresses)
MM = mass matrix (defines inertia)
β = Rayleigh damping coefficient that defines the damping ratio in terms of the stiffness matrix
$\overline{F}$ = time-dependent applied external forces

It can be shown that if the desired damping ratio is γ, then for an angular excitation frequency ω one should use (Smith and Griffiths, 1998):

$$\beta = \frac{2\gamma}{\varpi} \tag{5}$$

It should be noted that it is also possible to define the damping in terms of the stiffness matrix, using a slightly different form for the coefficient.

For the case where we assume that a steady-state harmonic excitation at angular rate ω is employed, we define the time-dependent forces and motion in terms of their amplitudes via:

$$\overline{F}(t) = \overline{F}_o e^{i\varpi t} \tag{6}$$

$$\overline{u}(t) = \overline{u}_o e^{i\varpi t} \tag{7}$$

Substituting Equations (6) and (7) into Equation (4), we obtain:

$$(KM + i\beta\varpi KM - \varpi^2 MM)\overline{u}_o = \overline{F}_o \tag{8}$$

Equation (8) is a time-independent matrix equation for the displacement amplitudes in terms of the amplitudes of the applied forces and an assumed set of tissue properties. It is convenient to write this in the standard matrix equation form:

$$Ax = b \tag{9}$$

where A is the (complex) matrix involving the terms in parenthesis in Equation (8), b represents the (real) amplitude of the forces supplied at the surface, and x is the solution vector which is therefore also complex. Physically, the fact that x is complex arises from differences in phase between the displacements at different points within the solid. The variations in phase are caused by the effects of damping.

Actually, one ordinarily does not know the forces applied at the surface of the breast but rather the magnitude of the forced oscillations. For this reason, Equation (9) is rewritten in practice so that the surface nodes are forced to have a known amplitude of vibration. One simple way to do this is to replace the associated matrix elements in Equation (9) as follows:

$$A_{ik} = \delta_{ik} \text{ (for i equal to externally excited degrees-of-freedom)} \tag{10}$$

$$b_k = \text{amplitude of excitation of k}^{\text{th}} \text{ degree-of-freedom} \qquad (11)$$

The terms in b corresponding to non-externally forced nodes are zero.

A difficult aspect of this problem is obtaining a solution of the matrix Equation (8) or (9). This solution is somewhat complicated in this case because the large matrix A, while sparse, is complex, usually symmetric, and therefore not Hermitian (i.e., $A \neq A^+$).

A direct solution scheme is available for equations of the form of (9) that takes advantage of the symmetry of A (Harwell, undated). This is a specialization of the typical LU-decomposition scheme ordinarily used to solve real matrix equations of the form (8). An advantage of such schemes is that once the matrix A has been decomposed, e.g., factored into lower- and upper-triangular matrices L and U, solutions for different forcing vectors b can be obtained with virtually no additional effort. This is useful for calculating the gradients, as demonstrated below.

However, for very large models, so-called "mesh-free" techniques are attractive, especially when coupled to iterative matrix solution techniques (Smith and Griffiths, 1998). The advantage of this scheme is that the complete stiffness and mass matrices MM and KM need never be assembled into memory, even in a sparse format. This allows very large problems to be solved even when memory is relatively limited. Good results were obtained in our case solving Equation (9) using a variant of the preconditioned conjugate gradient technique (PCG), namely the biconjugate gradient squared iterative method (Joubert, et al. undated). For example, the solution of a 20,000 element grid with 20,000 nodes was obtained in less than one and one-half minutes on a 400 MHz personal computer.

One problem was encountered using the iterative solution technique. Strangely, convergence of these techniques can be adversely affected if one begins the iteration process with a solution that is close to the correct one. This is potentially a serious disadvantage, since when performing the inverse problem one usually has an excellent approximation to the correct solution and use should be made of this to accelerate convergence. That is, if only a small change in Young's modulus is made, the previously converged results will be very close to the new ones. This problem was solved by calculating the change in displacements from the previous solution. Let A be the matrix for which a converged solution x has been obtained for a constant forcing function b. Let δA be the change caused by altered assumptions on Young's modulus. The change in the solution, δx, is given by:

$$(A + \delta A)(x + \delta x) = b \qquad (12)$$

The previous converged solution satisfied Equation (9). Subtracting Equation (9) from Equation (12) and keeping only the first order terms, we have:

$$A \delta x = -\delta A x \qquad (13)$$

The advantage of this formulation is that the iteration process can begin with $\delta x = 0$, which is required for good convergence with the PCG method, but the process completes much quicker

since the required accuracy in δx is much smaller than is needed for the complete solution $x + \delta x$.

An exact solution of the displacements is available for the special case of a rectangular solid, fixed on all but one edge and subjected to a transverse excitation whose amplitude varies sinusoidally across the unfixed edge (Gao, 1995). This solution was compared to the predictions of the finite element code. The latter involved a 10 cm x 10 cm square, modeled using 1 mm x 1 mm 3-node triangular elements. Figure 1 shows the displacement amplitude parallel to the direction of excitation down the midline of the solid. The code results agree reasonably well with the exact solution. It is noteworthy that the value of the damping ratio used in this example problem ($\xi = 0.1$) is not quite sufficient to prevent some standing waves from developing along the side of the rectangle that is opposite the driven edge.

Of course, the accuracy of the solution is controlled by the fineness of the grid and the fidelity afforded by the various types of elements. Figure 1 utilized a fairly coarse mesh, and more accurate solutions can be obtained by using more elements, quadrilateral elements instead of 3-node triangles, or triangles with more than 3 nodes. Figure 2 shows the behavior of a snapshot of the displacements at a particular time, i.e., the real part of the complex displacements (not their total amplitude as shown in Figure 1). The cases with a finer mesh (i.e., more nodes) show much better agreement with the exact solution.

Finally, the solutions obtained with the finite element model developed on this project were compared to those obtained with ANSYS. Good agreement was also obtained in these cases.

2.3.2 Calculation of the Gradient of the Displacement Figure-of-Merit

As discussed previously, given a set of measured (or simulated) displacement data, one must adjust the assumed Young's moduli to make the calculated displacements agree with the measured values. This can be formulated as an optimization problem, in which a measure of the disagreement is minimized. A common measure is the figure-of-merit shown in Equation (1).

Most efficient and robust techniques for minimizing functions of the form of Equation (1) require information on the change in the predicted displacements caused by a small change in input parameters. For example, the Levenberg-Marquardt technique requires extensive information that is time-consuming to calculate, i.e., the terms shown in Equation (2). The BFGS technique requires less gradient information, but it is still critical to develop this information in an efficient manner. For example, the crudest approach to calculate the gradient terms shown in Equation (3) would involve making a small change in a single modulus E_k and then recalculating the entire displacement solution. Repeating this process p times to calculate all such terms would again require a time on the order of p times n^3 or roughly n^4. In other words, this brute-force process would require the same length of time as the Levenburg-Marquardt method.

Note that the brute-force technique calculates the change in each displacement caused by a change in the input Young's moduli. Since we then sum over these displacements to calculate the figure-of-merit J, we see that the brute-force technique calculates much more information than we really need for BFGS. A better scheme is to use an adjoint technique that efficiently

7

calculates only the needed information (Kenton, 1981). If we have a set of algebraic equations of the form:

$$0 = g_i(x) \tag{14}$$

together with a single figure-of-merit $J(x)$, one defines an adjoint x^+ associated with each variable x by constructing the following equations:

$$0 = \sum_k \frac{\partial g_k}{\partial x_i} x_k^+ + \frac{\partial J}{\partial x_i} \tag{15}$$

After the terms x^+ have been calculated using Equation (15), the terms of Equation (3) can be obtained very simply by calculating the following sums:

$$\frac{\partial J}{\partial E_k} = \sum_i \frac{\partial g_i}{\partial E_k} x_i^+ \tag{16}$$

In our case, Equations (14) are linear, and the matrix terms in Equation (15) put into the standard form of Equation (9) are of the form:

$$A_{ik} = \frac{\partial g_k}{\partial x_i} = KM_{ki} + i\beta\varpi KM_{ki} - \varpi^2 MM_{ki} \tag{17}$$

Since the stiffness and mass matrices KM and MM are symmetric (Smith and Griffiths, 1998), the matrix A^t used to solve for the adjoints is the same as the matrix A used to solve for the displacements.

This symmetry offers the potential for a still larger savings in computation time, if sufficient memory is available to use direct sparse matrix techniques rather than an iterative scheme such as PCG. If we use such a direct matrix solution technique, we will manipulate A in some fashion (e.g., decompose it into upper- and lower-diagonal matrices) that will then allow the matrix equation to be readily solved. The time-consuming part of the solution process is the matrix manipulation step, which takes a time on the order of the cube of the rank, i.e., in this case n^3. The subsequent "back-substitution" process needed to obtain the solution x for a given b takes, by contrast, only a time on the order of n^2. Thus, direct methods are very appealing when used with the BFGS algorithm: after the matrix A has been manipulated to obtain a solution of the displacements, the adjoints can be obtained with the same matrix decomposition in essentially negligible additional time. The gradient terms are then obtained trivially using Equation (16).

2.3.3 Determining Young's Modulus from Displacements

The finite element code was augmented to calculate the gradient terms after the displacements were calculated using the adjoint method. The change in figure-of-merit caused by a change in one or more of the Young's moduli calculated using brute-force techniques was

found to agree very well with the results of the adjoint method. The gradient information was then used to minimize the figure-of-merit Equation (1). We tried several algorithms to achieve this, and the best results were obtained using a commercially-available implementation of the BFGS algorithm (IMSL, 1994). Figure 3 shows the relative rate at which the figure-of-merit converged in a typical problem (a value of zero for the figure-of-merit implies perfect convergence).

Figure 4 shows the Young's modulus obtained from computer-generated MRI displacement data. Computer-generated data were obtained by merely running the finite element code for a specified Young's modulus distribution, in this case a uniform distribution with a scaled value of 1 except for a square "tumor" of value 10 in the upper-right-hand corner. The minimization procedure then begins with a uniform (and incorrect) Young's modulus assumption, and iterates until the desired accuracy is obtained. As can be seen in Figure 4, the algorithm does an excellent job inferring Young's modulus from the computer-generated displacement data. This simulation required approximately 12 hours of computer time on a relatively slow 400 MHz personal computer. Numerous possibilities for increasing the speed of this procedure are available and will be addressed in the next phase of the project.

One detail of the algorithm needs to be clarified. Initial numerical experiments resulted in a much poorer reconstruction of the Young's modulus than is shown in Figure 4. Inevitably, we found that the method converged on a solution that involved non-physical (negative) Young's moduli adjacent to the "tumor." Further, the calculated Young's moduli inside the tumor boundary compensated for this and were too large. Other numerical artifacts involving negative Young's moduli also sometimes appeared near the boundary of the simulated breast. To solve these problems without instituting the full complication of a constrained minimization approach, the Young's moduli were mapped to a new variable α, and convergence was obtained on α. The mapping used:

$$E_k = E_{\min} + \alpha_k^2 \qquad (18)$$

guarantees that the Young's modulus will be larger than some physically-based minimum value E_{min}. This modification to the algorithm proved very beneficial.

2.4   IMPORTANCE OF POISSON'S RATIO

2.4.1   The Effect of Poisson's Ratio on Compressibility and Sound Speed

The example shown above used prototypical values of the Young's modulus for normal breast tissue and for tumors. However, the value of Poisson's ratio v was 0.3, a typical value for structural (non-biological) materials. To see what the appropriate values are for biological tissues, it is helpful to consider the speed of longitudinal and shear vibrations in tissue. These can be shown to be:

$$c_L^2 = \frac{E(1-v)}{\rho(1-2v)(1+v)} \qquad (19)$$

$$c_s^2 = \frac{E}{2\rho(1+v)} \tag{20}$$

The value for the Young's modulus E of normal breast tissue is on the order of 10,000 Pa (van Houten et al. [1999] use 8000 Pa). The density of tissue is about that of water, so ρ ~1000 kg/m^3. The speed of longitudinal vibrations c_L is just the sound speed, which is about 1500 m/sec. Using Equation (19), we can readily determine that Poisson's ratio must be very close to 0.5, so that Equation (19) simplifies to:

$$c_L^2 \cong \frac{E}{3\rho(1-2v)} \tag{21}$$

Equation (21) implies that $v \sim 0.499999$.

It is interesting to note that while the modulus E varies over a reasonably wide range, the sound speed is found to be quite constant, even in tumors (this is why ultrasound is only of limited use for detecting breast cancer). Equation (21) thus implies that Poisson's ratio must vary <u>slightly</u> as E varies to keep c_L constant.

Again following Smith and Griffiths (1998), the stiffness matrix KM is developed from a set of constitutive equations that relate strains ε to stresses σ. In the plane strain approximation, the associated matrix equation is written:

$$\sigma = D\varepsilon \tag{22}$$

where D has terms of the form

$$\frac{v}{1-v} \tag{23}$$

Thus, as v approaches 0.5, this matrix becomes ill-conditioned. Special techniques must be used to obtain a converged solution, which in any case can be difficult. In the limit where the Poisson's ratio becomes 0.5, the material becomes incompressible, the longitudinal sound speed becomes infinite, and an entirely different formulation of the equations of motion becomes necessary. In this formulation, an additional variable must be introduced, the hydrostatic pressure.

Most finite element codes are incapable of handling the purely incompressible case, and may have difficulties with the nearly-incompressible case as well. Numerical experiments with the Creare-built code showed poor convergence properties as Poisson's ratio was increased to 0.499 and above. Presumably for the same reason, some of the MRE work reported in the literature utilized a value of 0.49 (van Houten, 1999). At first glance, using 0.49 instead of 0.49999 . . . appears fairly reasonable, until one calculates the sound speeds. At a value of 0.49, for the Young's modulus and density cited earlier, Equations (19) and (20) yield:

$$c_L \approx 13 m/\sec \tag{24}$$

$$c_s \approx 1.8m/\text{sec} \tag{25}$$

Note that the longitudinal sound speed is far less than the actual value of ~1500 m/sec. Note also from Equation (20) that the shear speed is well-behaved as v approaches 0.5.

At an assumed excitation frequency of 200 Hz, in the range typical of MRE experiments, the corresponding wavelengths are given by the quotient of the sound speed and the frequency, yielding:

$$\lambda_L \approx 6.5cm \tag{26}$$

$$\lambda_s \approx 0.9cm \tag{27}$$

The shear wavelength is comparable to the size of the tumors. As mentioned earlier, achieving small wavelengths at the low frequencies resolvable by MRI is the advantage of using shear waves in the first place. However, the longitudinal wavelength has been made much shorter than the actual value at 200 Hz of about 7 meters. In effect, the use of a Poisson's ratio of 0.49 has made the tissue much more compressible than it actually is.

2.4.2 Investigative Calculations with ANSYS

To investigate the implications of using an artificially reduced value of Poisson's ratio, we performed a series of calculations with ANSYS. This code was used rather than the Creare code since the former more capably handles nearly-incompressible substances. The simulated "breast" in these calculations is a square of dimension 100 mm x 100 mm, excited along the upper edge with a forced displacement whose amplitude varies sinusoidally from zero at the left and right corners to a maximum value of 1 mm in the middle. In all cases, the excitation frequency is 200 Hz, the damping constant β is .00016 (Gao, 1995), and the density ρ is 1000 kg/m^3. The nominal modulus E is 10000 Pa.

These various cases are discussed below.

Case1: Nominal Case

The nominal case involves a homogeneous material, i.e., a stiff inclusion representing a tumor has not been included. The Poisson's ratio has been set to a value very close to 0.5 that will yield the proper longitudinal sound speed. The "breast" is excited in the up- and down-direction along the upper edge.

A "snapshot" of the calculated displacement amplitudes at a particular time is shown in Figure 5. The wavelength of the longitudinal waves are much larger than the 10 cm maximum dimension of the breast. Also, there are no inclusions that could possibly cause mode conversion from longitudinal to shear waves. Thus, no "waves" are seen, just positive amplitude displacements in the y-direction.

11

Case 2: Shear Excitation

This is the same as Case 1, except that the breast is excited in the x- (shear) direction. In this case, Figure 6 reveals shear waves with the expected wavelength of about 0.9 cm, that are damped fairly quickly with depth. Note that the black box shown in the figure has no significance in this case (the box denotes the location of the inclusion when one is used in Case 4).

Case 3: Artificially Reduced Poisson's Ratio with Longitudinal Excitation

This is the same as Case 1, i.e., there is still no stiff inclusion and the breast is excited in the vertical direction, but in this case a reduced Poisson's ratio of 0.49 is used as in some previously published research. Figure 7 exhibits longitudinal waves with a wavelength of roughly 6.5 cm as expected from Equation (26). The comparison of Figure 7 with Figure 5 clearly illustrates the deleterious effects of using too small a value for Poisson's ratio.

Case 4: Correct Poisson's Ratio, Stiff Inclusion, Shear-Excitation

This case is similar to Case 2 in that it employs the correct Poisson's ratio. Also, in this case a stiff inclusion is provided at the location of the dark box. The stiffness (increased Young's modulus) of the inclusion leads to an increase in sound speed. The corresponding increase in shear wavelength can be seen in Figure 8. The evident distortions in the wave patterns provide the raw data necessary for an inverse method to estimate the Young's modulus.

2.4.3 Conclusions of Poisson's Ratio Investigations

The assumed Poisson's ratio exhibits a profound effect on the displacement patterns. While the use of a reduced value (e.g., 0.49) greatly assists in numerical convergence, this cannot be recommended since it gives rise to relatively low longitudinal wave speeds, correspondingly short wavelengths, and substantial distortion of the calculated displacements. An intriguing question is whether this effect may partly explain the artifacts reported in the literature when in vivo data and that from phantoms are used. To date, these problems have been attributed to the use of plane strain approximation or linear materials models. If more detailed, 3-D viscoelastic models are needed, this will further exacerbate the problems of long-running inverse calculations for any future clinical applications, so it would be useful to resolve this question.

Since the longitudinal wavelengths at the frequencies of interest are much larger than the breast, it appears entirely justified to use a completely incompressible formulation if this will improve numerical performance. This should eliminate the numerical problems associated with modeling nearly-incompressible behavior. Such an approach was previously recommended by Skovoroda et al. (1995).

2.5 PLANS FOR THE SECOND YEAR OF THE PROJECT

During the second year of the project, we plan to implement an incompressible formulation of the tissue equations of motion in the Creare code. We anticipate that this will eliminate the numerical problems associated with the use of a Poisson's ratio near 0.5. We also plan to undertake efforts to further improve the already relatively fast execution speed. Finally, we will also attempt to obtain existing measured MRI displacement data for a phantom from a

cooperating institution. Using these data, we will attempt to reconstruct the Young's modulus distribution and compare it to the known values.

3.0   KEY RESEARCH ACCOMPLISHMENTS

- An adjoint method developed on this project provides an extremely efficient technique for calculating the gradient of the goodness-of-fit measure that is the basis of the inverse algorithm.

- Combining the adjoint method with the BFGS algorithm provides an efficient means for calculating tissue stiffness from MRI displacement data.

- Much of the experience with Magnetic Resonance Elastography previously reported in the literature has utilized an incorrect value of Poisson's ratio.

- Use of an incorrect Poisson's ratio leads to a drastic underprediction of the longitudinal acoustic wavelength, which in turn can be expected to cause artifacts in the reconstructed hardness values.

4.0   REPORTABLE OUTCOMES

There were no reportable outcomes in the first year of the project.

5.0   CONCLUSIONS

Magnetic Resonance Elastography is potentially a very effective tool for the early diagnosis of breast cancer. The lack of an efficient and robust means for solving the inverse problem is the most challenging technical problem preventing widespread clinical use of MRE. During the first year of the project, we have developed and demonstrated a new, highly efficient algorithm for solving the inverse problem. The results obtained so far with this algorithm are very promising. We have also determined that poor MRE results reported in the literature may have been partly caused by using incorrect values for the Poisson's ratio of breast tissue. During the next year, we will develop a mathematically-robust algorithm that will allow more accurate modeling of tissue motion during MRE.

6.0   REFERENCES

T. L., Chenevert, A. R. Skovoroda, M. O'Donnell, S. Y. Emelianov, Elasticity Reconstructive Imaging via Stimulated Echo MRI, *Magnetic Resonance In Medicine* 39 (1998).

L. Gao, Sonoelastography: Theory and Experriment Development, PhD thesis (University of Rochester, 1995).

Harwell Sparse Matrix Package, procedure ME47 (undated).

W. D. Joubert, Y. Shen, S. Swift, Getting Started with PCG, Version 1.0 (Los Alamos National Laboratory, undated).

M. A. Kenton, A General Sensitivity Theory for Simulations of Nonlinear, Time-Dependent Systems, Cornell University Reactor Laboratory, report CURL-58 (January 1981).

A. Manduca, R. Muthupillai, P. J. Rossman, J. F. Greenleaf, R. L. Ehman, Image Processing for Magnetic Resonance Elastography, SPIE 2710, 616-623 (1996).

R. Muthupillai, R. L. Ehman, R.L., Magnetic Resonance Elastography, *Nature* 2, 5 (May 1996).

R. Muthupillai, D. J. Lomas, P. J. Rossman, J. F. Greenleaf, A. Manduca, R. L. Ehman, Magnetic Resonance Elastography by Direct Visualization of Propagating Acoustic Strain Waves, *Science* 269 (September 29, 1995).

W. H. Press, B. P. Flannery, S. A. Teukolsky, W. T. Vetterling, *Numerical Recipes*, Cambridge University Press (1986).

K. R. Raghavan, A. E. Yagle, Forward and Inverse Problems in Elasticity Imaging of Soft Tissues, *IEEE Trans. Nuclear Science* 41, 4 (August 1994).

A. R. Skovoroda, S. Y. Emelianov, M. O'Donnell, Tissue Elasticity Reconstruction Based on Ultrasonic Displacement and Strain Images, *IEEE Transactions on Ultrasonics, Ferroeleectris, and Frequency Control* 42, 4 (July 1995).

I. M. Smith and D.V. Griffiths, *Programming the Finite Element Method*, Third Edition, John Wiley (April 1998).

G. Trahey, remarks made during discussion of paper 4325-14, K. Nightingale, M-S Soo, R. Nightingale, M. Palmeri, G. Trahey, Investigation of Real-time Remote Palpation Imaging, Medical Imaging 2001, SPIE, San Diego (2001).

E. E. W. Van Houten, K. K. Paulsen, M. I. Miga, F. E. Kennedy, J. B. Weaver, An Overlapping Subzone Technique for MR-Based Elastic Property Reconstruction, *Magnetic Resonance in Medicine* 42, 779-786 (1999).

E. E. W. Van Houten, K. D. Paulsen, M. I. Miga, F. E. Kennedy, J. B. Weaver, A Subzone Based Nonlinear Inversion Scheme for Viscoelastic Tissue Properties, Medical Imaging 2000: Image Processing, Proc. SPIE Vol. 3979 (2000b).

E. E. W. Van Houten, J. B. Weaver, M. I. Miga, F. E. Kennedy, K. D. Paulsen, Elasticity Reconstruction from Experimental MR Displacement Data: Initial Experience with an Overlapping Subzone Finite Element Inversion Process, *Med. Phys* 27, 1 (January 2000a).

T. Wu, J. P. Felmlee, J. F. Greenleaf, S. J. Riederer, R. L. Ehman, MR Imaging of Shear Waves Generated by Focused Ultrasound, *Magnetic Resonance in Medicine* 43, 111-115 (2000).
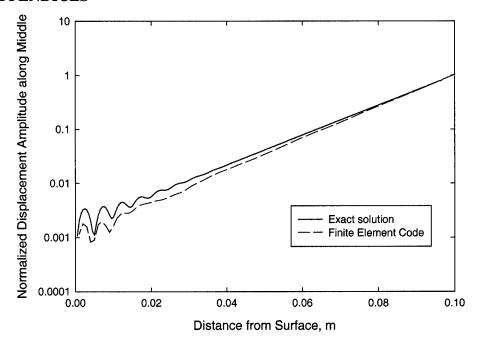
7.0 APPENDICES

Figure 1. Comparison of Finite Element Code Predictions of the Logarithm of the Displacement Amplitude to the Logarithm of the Displacement Amplitude for the Exact Solution. These data show that our finite element code closely matches the exact solution for the analyzed configuration.
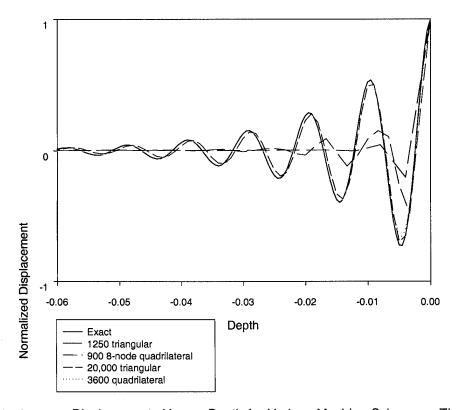

Figure 2. Instantaneous Displacements Versus Depth for Various Meshing Schemes. These data show the effect of model order on the match to the exact solution. For this model, 3600 quadrilateral elements or 20,000 triangular elements yield good model accuracy.
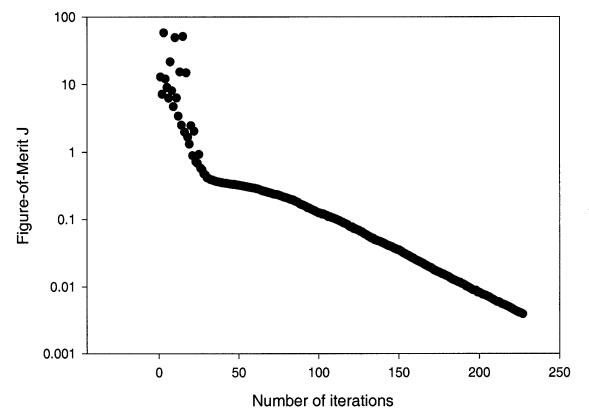
Figure 3. Convergence Rate of BFGS Algorithm. These data show that the figure of merit accuracy improves exponentially (linearly on a log scale) with the number of iterations.
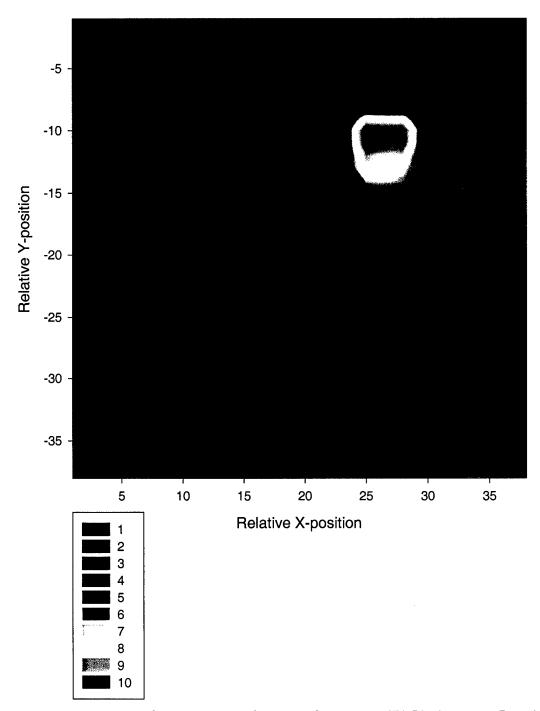
Reconstructed Young's Modulus

Figure 4. Young's Modulus Calculated from Computer-Generated MRI Displacement Data Using the Creare Code and Algorithm. The stiffness (relative modulus 10) of the simulated tumor in the upper-right-hand corner can be easily discerned.
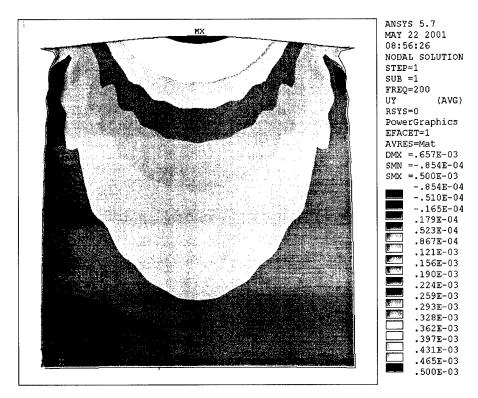
ANSYS 5.7
MAY 22 2001
08:56:26
NODAL SOLUTION
STEP=1
SUB =1
FREQ=200
UY   (AVG)
RSYS=0
PowerGraphics
EFACET=1
AVRES=Mat
DMX =.657E-03
SMN =-.854E-04
SMX =.500E-03
     -.854E-04
     -.510E-04
     -.165E-04
      .179E-04
      .523E-04
      .867E-04
      .121E-03
      .156E-03
      .190E-03
      .224E-03
      .259E-03
      .293E-03
      .328E-03
      .362E-03
      .397E-03
      .431E-03
      .465E-03
      .500E-03

Figure 5. Calculated Longitudinal Displacements for the Nominal Case (longitudinal excitation) for Correct Material Properties Using ANSYS.

ANSYS 5.7
MAY 24 2001
08:53:46
NODAL SOLUTION
STEP=1
SUB =1
FREQ=200
UX   (AVG)
RSYS=0
PowerGraphics
EFACET=1
AVRES=Mat
DMX =.500E-03
SMN =-.309E-03
SMX =.500E-03
     -.309E-03
     -.262E-03
     -.214E-03
     -.167E-03
     -.119E-03
     -.714E-04
     -.238E-04
      .238E-04
      .714E-04
      .119E-03
      .167E-03
      .214E-03
      .262E-03
      .309E-03
      .357E-03
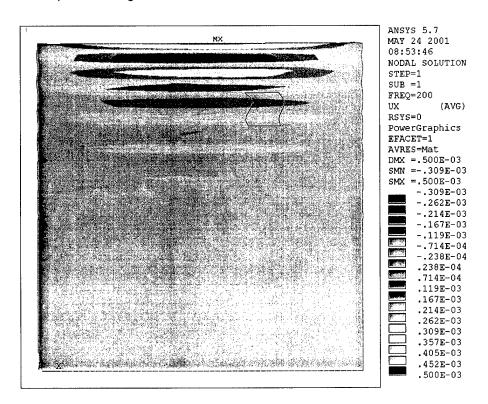   .405E-03
      .452E-03
      .500E-03

Figure 6. Calculated Shear Displacements for Shear Excitation with Correct Material Properties Using ANSYS.
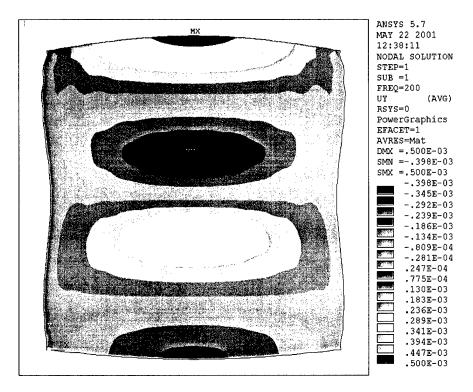
Figure 7. Calculated Longitudinal Displacement for Longitudinal Excitation with Artificially Lowered Poisson's Ratio Using ANSYS.
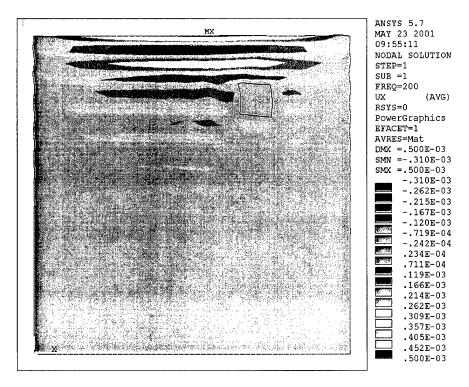

Figure 8. Calculated Shear Displacements for Shear Excitation with Correct Material Properties Using ANSYS with Stiff Inclusion.